ЖУРНАЛ ФІЗИЧНИХ ДОСЛІДЖЕНЬ
т. 22, № 2 (2018) 2702(12 с.)

JOURNAL OF PHYSICAL STUDIES
v. 22, No. 2 (2018) 2702(12 p.)

# INFLUENCE OF UNIAXIAL PRESSURES ON DYNAMIC PROPERTIES OF $NH_3CH_2COOH{\cdot}H_2PO_3$ FERROELECTRIC

I. R. Zachek[1], R. R. Levitskii[2], A. S. Vdovych[2]
[1] *Lviv Polytechnic National University, 12, Bandera St., Lviv, UA–79013, Ukraine*
[2] *Institute for Condensed Matter Physics of the National Academy of Sciences of Ukraine, 1, Svientsitskii St., Lviv, UA–79011, Ukraine*
(Received 06 Febrary, 2018; in final form — 14 May, 2018)

Using a modified model of $NH_3CH_2COOH{\cdot}H_2PO_3$ ferroelectric by taking into account the piezoelectric coupling with strains $\varepsilon_i$ within the Glauber method in a two-particle cluster approximation, the system of kinetic equations for mean values of pseudospins has been obtained. On the basis of the solutions of these equations we obtained the expressions for the components of the dynamic dielectric permittivity tensor of GPI and the relaxation times of the model. The influence of uniaxial pressures on these characteristics at different temperatures and frequencies have been studied.

**Key words**: ferroelectrics, dielectric permittivity, relaxation time, uniaxial pressure.

DOI: https://doi.org/10.30970/jps.22.2702

PACS number(s): 77.22.−d, 77.22.Ch, 77.22.Ej, 77.22.Gm

## I. INTRODUCTION

An attempt to shed light onto the $NH_3CH_2COOH{\cdot}H_2PO_3$ (GPI) phase transition mechanism is the main motivation for the studies that we proposed last year. Our aim is to develop a pseudospin model of a GPI crystal, which can describe the experimentally observed temperature, frequency, field and pressure dependences of the thermodynamic and dynamic characteristics of such crystal. While constructing such a model, we must take into consideration the structural feature of hydrogen bonds in GPI and find out how the phase transition in the crystal relates to proton ordering on the O–H...O hydrogen bonds, which connect the phosphite groups $HPO_3$ into chains along $c$-axis of the crystal. All other structural changes in these materials are considered by us through effective model parameters.

The autors of [1] we proposed the proton ordering model of GPI which explains the temperature dependence of the dielectric permittivity of GPI. In [2] this model is modified by taking into account the piezoelectric coupling of ordering structure elements with strains $\varepsilon_i$. Within a two-particle cluster approximation, the polarization vector, the components of the dielectric permittivity tensor for mechanically free and clamped crystals, their piezoelectric and thermal characteristics are calculated. At the proper set of theory parameters, a good quantitative description of the available experimental data for these characteristics was obtained. On the basis of this model, we succeeded in producing a quantitatively right description of electric field effects [3] and the effects of hydrostatic [4] and uniaxial [5] pressures on the physical characteristics of GPI.

In [6], on the basis of model [2], using the Glauber approach we succeeded in describing the dynamic dielectric permittivity tensor for a mechanically clamped GPI crystal. In the present paper, the approach proposed in [6] is used for the study of the influence of uniaxial pressures on the dynamic dielectric permittivity of GPI.

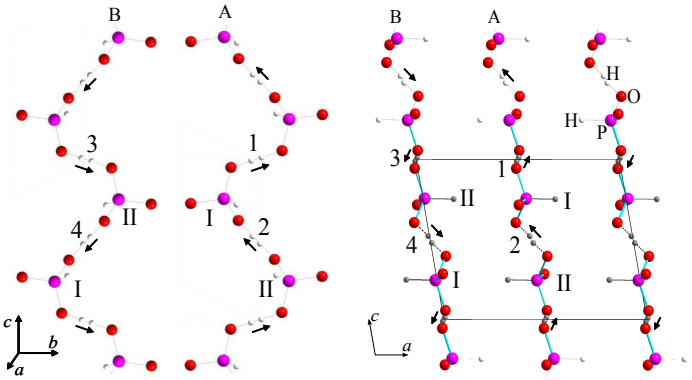


Fig. 1. The orientations of vectors $\mathbf{d}_{qf}$ in the primitive cell in the ferroelectric phase [2, 3].

## II. THE MODEL OF A GPI CRYSTAL

In the paraelectric phase, a GPI crystal crystalizes in a monoclinic $P2_1/a$ space group. At the temperature 225 K, the crystal transits to a ferroelectric state (space group $P2_1$) with the spontaneous polarization along crystallographic $b$-axis (Fig. 1). The pseudospin model proposed in [1] considers the system of protons in GPI, localised on O-H...O bonds with a double-well potential between phosphite groups $HPO_3$, which form chains along the crystalographic $c$-axis. Dipole moments $\mathbf{d}_{qf} = \boldsymbol{\mu}_f \frac{\sigma_{qf}}{2}$ are ascribed to the protons on the bonds. Here $q$ is the number of primitive cell, $f = 1, \ldots, 4$; $\frac{\sigma_{qf}}{2}$ are pseudospin variables that describe the changes connected with the reorientation of the dipole moments.

The Hamiltonian of the model at applied electric fields $E_1$, $E_2$, $E_3$ along positive directions of the Cartesian ax-

es $X$, $Y$ and $Z$ ($X \perp (b,c)$, $Y \parallel b$, $Z \parallel c$) can be written as follows:

$$\hat{H} = NU_{\text{seed}} + \hat{H}_{\text{short}} + \hat{H}_{\text{long}} + \hat{H}_E, \tag{2.1}$$

where $N$ is the total number of primitive cells. The first term in (2.1) is the "seed" energy, which relates to the heavy ion sublattice and does not depend explicitly on the configuration of the proton subsystem. It includes the elastic, piezolectric and dielectric parts, expressed in terms of electric fields $E_i$ and strains $\varepsilon_i$:

$$U_{\text{seed}} = v\Big(\frac{1}{2}\sum_{j,j'=1}^{6} c_{jj'}^{E0}(T)\varepsilon_j\varepsilon_{j'} - \sum_{i=1}^{3}\sum_{j=1}^{6} e_{ij}^{0}\varepsilon_j E_i - \sum_{i,i'=1}^{3}\frac{1}{2}\chi_{ii'}^{\varepsilon 0}E_iE_{i'}\Big). \tag{2.2}$$

Parameters $c_{ij}^{E0}(T)$, $e_{ij}^{0}$, $\chi_{ij}^{\varepsilon 0}$ are so called "seed" elastic constants, piezoelectric stresses and dielectric susceptibilities, respectively; $v$ is the volume of a primitive cell.

The second term in (2.1) is the Hamiltonian of short-range interactions:

$$\hat{H}_{\text{short}} = 2w\sum_{qq'}\Big(\frac{\sigma_{q1}}{2}\frac{\sigma_{q2}}{2}+\frac{\sigma_{q3}}{2}\frac{\sigma_{q4}}{2}\Big) \times \big(\delta_{\mathbf{R}_q\mathbf{R}_{q'}} + \delta_{\mathbf{R}_q+\mathbf{R_c},\mathbf{R}_{q'}}\big). \tag{2.3}$$

In (2.3) $\sigma_{qf}$ is the $z$-component of the pseudospin operator, that describes the state of the $f$-th bond ($f = 1,2,3,4$) in the $q$-th cell. The first Kronecker delta corresponds to the interaction between the protons in the chains near the tetrahedra $HPO_3$ of type "I" (Fig. 1), while the second near the tetrahedra $HPO_3$ of type "II", $\mathbf{R_c}$ is the lattice vector along the crystallographic $c$-axis. Parameter $w$, which describes the short-range interactions within the chains, is expanded linearly into series over strains $\varepsilon_i$:

$$w = w^0 + \sum_{i=1}^{6}\delta_i\varepsilon_i. \tag{2.4}$$

The third term in (2.1) describes the long-range dipole-dipole interactions and indirect (through the lattice vibrations) interactions between protons, which are taken into account in the mean field approximation:

$$\hat{H}_{\text{long}} = \frac{1}{2}\sum_{\substack{qq'\\ff'}} J_{ff'}(qq')\frac{\langle\sigma_{qf}\rangle}{2}\frac{\langle\sigma_{q'f'}\rangle}{2} - \sum_{\substack{qq'\\ff'}} J_{ff'}(qq')\frac{\langle\sigma_{q'f'}\rangle}{2}\frac{\sigma_{qf}}{2}. \tag{2.5}$$

The fourier transforms of the interaction constants $J_{ff'} = \sum\limits_{q'} J_{ff'}(qq')$ at $\mathbf{k} = 0$ are linearly expanded over the strains $\varepsilon_i$:

$$J_{ff'} = J_{ff'}^0 + \frac{\partial J_{ff'}}{\partial\varepsilon_i}\varepsilon_i = J_{ff'}^0 + \sum_{i=1}^{6}\psi_{ff'i}\varepsilon_i. \tag{2.6}$$

As a result, (2.5) can be written as:

$$\hat{H}_{long} = NH^0 - \sum_{q}\sum_{f=1}^{4}\mathcal{H}_f\frac{\sigma_{qf}}{2}, \tag{2.7}$$

where

$$H^0 = \frac{1}{8}J_{11}(\eta_1^2+\eta_3^2) + \frac{1}{8}J_{22}(\eta_2^2+\eta_4^2) + \frac{1}{4}J_{13}\eta_1\eta_3 + \frac{1}{4}J_{24}\eta_2\eta_4 + \frac{1}{4}J_{12}(\eta_1\eta_2+\eta_3\eta_4) + \frac{1}{4}J_{14}(\eta_1\eta_4+\eta_2\eta_3), \quad \eta_f = \langle\sigma_{qf}\rangle. \tag{2.8}$$

In (2.7) the notations are used:

$$\begin{aligned}
\mathcal{H}_1 &= \frac{1}{2}J_{11}\eta_1 + \frac{1}{2}J_{12}\eta_2 + \frac{1}{2}J_{13}\eta_3 + \frac{1}{2}J_{14}\eta_4,\\
\mathcal{H}_2 &= \frac{1}{2}J_{22}\eta_2 + \frac{1}{2}J_{12}\eta_1 + \frac{1}{2}J_{24}\eta_4 + \frac{1}{2}J_{14}\eta_3,\\
\mathcal{H}_3 &= \frac{1}{2}J_{11}\eta_3 + \frac{1}{2}J_{12}\eta_4 + \frac{1}{2}J_{13}\eta_1 + \frac{1}{2}J_{14}\eta_2,\\
\mathcal{H}_4 &= \frac{1}{2}J_{22}\eta_4 + \frac{1}{2}J_{12}\eta_3 + \frac{1}{2}J_{24}\eta_2 + \frac{1}{2}J_{14}\eta_1.
\end{aligned} \tag{2.9}$$

The fourth term in (2.1) describes the interactions of pseudospins with an external electric field:

$$\hat{H}_E = -\sum_{qf}\boldsymbol{\mu}_f\vec{E}\frac{\sigma_{qf}}{2}. \tag{2.10}$$

Here $\boldsymbol{\mu}_1 = (\mu_{13}^x, \mu_{13}^y, \mu_{13}^z)$, $\boldsymbol{\mu}_3 = (-\mu_{13}^x, \mu_{13}^y, -\mu_{13}^z)$, $\boldsymbol{\mu}_2 = (-\mu_{24}^x, -\mu_{24}^y, \mu_{24}^z)$, $\boldsymbol{\mu}_4 = (\mu_{24}^x, -\mu_{24}^y, -\mu_{24}^z)$ are the effective dipole moments per one pseudospin.

The two-particle cluster approximation for short-range interactions and the mean field approximation for long-range interactions are used for the calculation of the thermodynamic characteristics of GPI. In this approximation thermodynamic potential is given by:

$$G = NU_{\text{seed}} + NH^0 - Nv\sum_{i=1}^{6}\sigma_i\varepsilon_i - k_{\text{B}}T\sum_{q}\Big\{2\ln\text{Sp}\,e^{-\beta\hat{H}_q^{(2)}} - \sum_{f=1}^{4}\ln\text{Sp}\,e^{-\beta\hat{H}_{qf}^{(1)}}\Big\}, \tag{2.11}$$

Here $\beta = 1/k_{\text{B}}T$, $k_{\text{B}}$ is the Boltzmann constant, $\hat{H}_q^{(2)}$, $\hat{H}_{qf}^{(1)}$ are two-particle and one-particle Hamiltonians:

$$\hat{H}_q^{(2)} = -2w\Big(\frac{\sigma_{q1}}{2}\frac{\sigma_{q2}}{2} + \frac{\sigma_{q3}}{2}\frac{\sigma_{q4}}{2}\Big) - \sum_{f=1}^{4}\frac{y_f}{\beta}\frac{\sigma_{qf}}{2}, \tag{2.12}$$

$$\hat{H}_{qf}^{(1)} = -\frac{\bar{y}_f}{\beta}\frac{\sigma_{qf}}{2}, \tag{2.13}$$

where such notations are used:

$$y_f = \beta(\Delta_f + \mathcal{H}_f + \boldsymbol{\mu}_f\mathbf{E}), \tag{2.14}$$

$$\bar{y}_f = \beta\Delta_f + y_f. \tag{2.15}$$

The symbols $\Delta_f$ are the effective cluster fields created by the neighboring bonds from the outside of the cluster. By minimizing the thermodynamic potential (2.11) with respect to the cluster fields $\Delta_f$ and the strains $\varepsilon_i$, and expressing $\Delta_f$ through the equilibrium order parameters $\tilde{\eta}_1 = \tilde{\eta}_3 = \tilde{\eta}_{13}$, $\tilde{\eta}_2 = \tilde{\eta}_4 = \tilde{\eta}_{24}$ we have obtained the system of equations for the equilibrium order parameters and strains in the case of zero mechanical stresses and fields:

$$\tilde{\eta}_{13} = \frac{1}{\widetilde{D}}[\sinh(\tilde{y}_{13} + \tilde{\eta}_{24}) + a^2 \sinh(\tilde{y}_{13} - \tilde{\eta}_{24}) + 2a \sinh \tilde{y}_{13}], \tag{2.16}$$

$$\tilde{\eta}_{24} = \frac{1}{\widetilde{D}}[\sinh(\tilde{y}_{13} + \tilde{\eta}_{24}) - a^2 \sinh(\tilde{y}_{13} - \tilde{\eta}_{24}) + 2a \sinh \tilde{\eta}_{24}],$$

$$-p_l = \sum_{i=1}^{6} c_{li}^{E0}\varepsilon_i - \frac{2\delta_l}{v} + \frac{2\delta_l}{v\widetilde{D}} M_\varepsilon - \frac{\psi_{1l}^{+}}{4v}\tilde{\eta}_{13}^2 - \frac{\psi_{2l}^{+}}{2v}\tilde{\eta}_{13}\tilde{\eta}_{24} - \frac{\psi_{3l}^{+}}{4v}\tilde{\eta}_{24}^2, \quad (l = 1, \ldots, 6), \quad p_4 = p_5 = p_6 = 0,$$

where such notations are used:

$$\tilde{y}_{13} = \frac{1}{2}\ln\frac{1+\tilde{\eta}_{13}}{1-\tilde{\eta}_{13}} + \beta\nu_1^{+}\tilde{\eta}_{13} + \beta\nu_2^{+}\tilde{\eta}_{24},$$

$$\tilde{y}_{24} = \beta\nu_2^{+}\tilde{\eta}_{13} + \frac{1}{2}\ln\frac{1+\tilde{\eta}_{24}}{1-\tilde{\eta}_{24}} + \beta\nu_3^{+}\tilde{\eta}_{24},$$

$$\nu_l^{\pm} = \nu_l^{0\pm} + \sum_{i=1}^{6}\psi_{li}^{\pm}\varepsilon_i,$$

$$\nu_1^{0\pm} = \frac{1}{4}(J_{11}^0 \pm J_{13}^0); \quad \psi_{1i}^{\pm} = \frac{1}{4}(\psi_{11i} \pm \psi_{13i}),$$

$$\nu_2^{0\pm} = \frac{1}{4}(J_{12}^0 \pm J_{14}^0); \quad \psi_{2i}^{\pm} = \frac{1}{4}(\psi_{12i} \pm \psi_{14i}),$$

$$\nu_3^{0\pm} = \frac{1}{4}(J_{22}^0 \pm J_{24}^0); \quad \psi_{3i}^{\pm} = \frac{1}{4}(\psi_{22i} \pm \psi_{24i}).$$

$$\tilde{D} = \cosh(\tilde{y}_{13} + \tilde{y}_{24}) + a^2\cosh(\tilde{y}_{13} - \tilde{y}_{24}) + 2a\cosh\tilde{y}_{13} + 2a\cosh\tilde{y}_{24} + a^2 + 1,$$

$$M_\varepsilon = 2a^2\cosh(\tilde{y}_{13} - \tilde{y}_{24}) + 2a\cosh\tilde{y}_{13} + 2a\cosh\tilde{y}_{24} + 2a^2,$$

$$a = e^{-\frac{1}{k_B T}\left(w^0 + \sum_{i=1}^{3}\delta_i\varepsilon_i + \sum_{j=4}^{6}\delta_j\varepsilon_j\right)}.$$

## III. THE RELAXATIONAL DYNAMICS OF A MECHANICALLY CLAMPED GPI CRYSTAL

For the calculations of dynamic properties we use the approach which is based on the ideas of thestochastic Glauber model [7]. Using the methods developed in [6,8], we obtain the following system of the Glauber equations for time dependent correlation functions of the pseudospins:

$$-\alpha\frac{d}{dt}\langle\prod_f \sigma_{qf}\rangle = \sum_{f'}\left\langle \prod_f \sigma_{qf}\left[1 - \sigma_{qf'}\tanh\frac{1}{2}\beta\varepsilon_{qf'}(t)\right]\right\rangle, \tag{3.1}$$

where parameter $\alpha$ determines the time scale of dynamic processes, $\varepsilon_{qf'}(t)$ is the local field acting on the $f'$-th pseudospin in $q$-th cell. We use a two-particle cluster approximation to obtain a closed system of equations. In this approximation, local fields $\varepsilon_{qf}(t)$ are coefficients at $\sigma_{qf}/2$ in a two-particle and a one-particle Hamiltonians (2.12) and (2.13). These fields are presented in a two-particle approximation

$$\begin{aligned} \varepsilon_{q1} &= w\sigma_{q2} + \frac{y_1}{\beta}, \ \varepsilon_{q2} = w\sigma_{q1} + \frac{y_2}{\beta} \\ \varepsilon_{q3} &= w\sigma_{q4} + \frac{y_3}{\beta}, \ \varepsilon_{q4} = w\sigma_{q3} + \frac{y_4}{\beta}, \end{aligned} \tag{3.2}$$

and in a one-particle approximation

$$\varepsilon_{qf} = \frac{\bar{y}_f}{\beta}.$$

As a result, from (3.1) we obtain the system of equations for the mean values of pseudospins $\langle\sigma_{qf}\rangle = \eta_f$ in a two-particle approximation

$$\begin{aligned} &\alpha\frac{d}{dt}\eta_1 = -\eta_1 + P_1\eta_2 + L_1, \ \alpha\frac{d}{dt}\eta_3 = -\eta_3 + P_3\eta_4 + L_3, \\ &\alpha\frac{d}{dt}\eta_2 = P_2\eta_1 - \eta_2 + L_2, \ \alpha\frac{d}{dt}\eta_4 = P_4\eta_3 - \eta_4 + L_4 \end{aligned} \tag{3.3}$$

and in a one-particle approximation as follows

$$\begin{aligned} &\alpha\frac{d}{dt}\eta_1 = -\eta_1 + \tanh\frac{\bar{y}_1}{2}, \ \alpha\frac{d}{dt}\eta_3 = -\eta_3 + \tanh\frac{\bar{y}_3}{2} \\ &\alpha\frac{d}{dt}\eta_2 = -\eta_2 + \tanh\frac{\bar{y}_2}{2}, \ \alpha\frac{d}{dt}\eta_4 = -\eta_4 + \tanh\frac{\bar{y}_4}{2}, \end{aligned} \tag{3.4}$$

where the following notations are used:

$$P_f=\frac{1}{2}\left[\tanh\left(\frac{\beta w}{2}+\frac{y_f}{2}\right)-\mathrm{th}\left(-\frac{\beta w}{2}+\frac{y_f}{2}\right)\right], \quad (3.5)$$

$$L_f=\frac{1}{2}\left[\tanh\left(\frac{\beta w}{2}+\frac{y_f}{2}\right)+\mathrm{th}\left(-\frac{\beta w}{2}+\frac{y_f}{2}\right)\right].$$

Let us confine ourselves to the case of small deviations from the equilibrium state for solving equations (3.3) and (3.4). For this case, we write $\eta_f$ and effective fields $y_f$, $\bar{y}_f$ in the form of a sum of equilibrium values and their deviations from the equilibrium values (a mechanically clamped crystal):

$$\eta_{1,3}=\tilde{\eta}_{13}+\eta_{1,3t}, \quad \eta_{2,4}=\tilde{\eta}_{24}+\eta_{2,4t}, \quad (3.6)$$

$$\begin{aligned} y_1&=\tilde{y}_{13}+y_{1t}=\beta\Delta_{13}+2\beta\nu_1\tilde{\eta}_{13}+2\beta\nu_2\tilde{\eta}_{24}\\ &+\Delta_{1t}+2\nu_{11}\eta_{1t}+2\nu_{12}\eta_{2t}+2\nu_{13}\eta_{3t}+2\nu_{14}\eta_{4t}\\ &+\mu^x_{13}E_{1t}+\mu^y_{13}E_{2t}+\mu^z_{13}E_{3t},\ E_{it}=E_ie^{i\omega t},\\ y_3&=\tilde{y}_{13}+y_{3t}=\beta\Delta_{13}+2\beta\nu_1\tilde{\eta}_{13}+2\beta\nu_2\tilde{\eta}_{24}\\ &+\Delta_{3t}+2\nu_{11}\eta_{3t}+2\nu_{12}\eta_{4t}+2\nu_{13}\eta_{1t}+2\nu_{14}\eta_{2t}\\ &-\mu^x_{13}E_{1t}+\mu^y_{13}E_{2t}-\mu^z_{13}E_{3t},\\ y_2&=\tilde{y}_{24}+y_{2t}=\beta\Delta_{24}+2\beta\nu_2\tilde{\eta}_{13}+2\beta\nu_3\tilde{\eta}_{24}\\ &+\Delta_{2t}+2\nu_{22}\eta_{2t}+2\nu_{12}\eta_{1t}+2\nu_{24}\eta_{4t}+2\nu_{14}\eta_{3t}\\ &-\mu^x_{24}E_{1t}-\mu^y_{24}E_{2t}+\mu^z_{24}E_{3t},\\ y_4&=\tilde{y}_{24}+y_{4t}=\beta\Delta_{24}+2\beta\nu_2\tilde{\eta}_{13}+2\beta\nu_3\tilde{\eta}_{24}\\ &+\Delta_{4t}+2\nu_{22}\eta_{4t}+2\nu_{12}\eta_{3t}+2\nu_{24}\eta_{2t}+2\nu_{14}\eta_{1t}\\ &+\mu^x_{24}E_{1t}-\mu^y_{24}E_{2t}-\mu^z_{24}E_{3t},\\ \bar{y}_f&=\beta\Delta_f+\tilde{y}_f+\beta\Delta_{ft}+y_{ft}. \end{aligned}$$

Here $\Delta_{13}=\Delta_1=\Delta_3$, $\Delta_{24}=\Delta_2=\Delta_4$ are equilibrium effective cluster fields, and $\Delta_{ft}$ are their deviations from equilibrium values. Parameters $\nu_i^{\pm}$ describe long-range interactions.

We decompose the coefficients $P_f$ and $L_f$ in a series of $\frac{y_{ft}}{2}$ limited by linear terms:

$$P_{1,3}=P^{(0)}_{13}+\frac{y_{1,3t}}{2}P^{(1)}_{13},\ L_{1,3}=L^{(0)}_{13}+\frac{y_{1,3t}}{2}L^{(1)}_{13}, \quad (3.7)$$
$$P_{2,4}=P^{(0)}_{24}+\frac{y_{2,4t}}{2}P^{(1)}_{24},\ L_{2,4}=L^{(0)}_{24}+\frac{y_{2,4t}}{2}L^{(1)}_{24},$$

where the following notations are used:

$$P^{(0)}_{13}=\frac{1-a^2}{Z_{13}}, \quad P^{(1)}_{13}=\frac{-4a(1-a^2)\sinh\tilde{y}_{13}}{Z^2_{13}},$$
$$L^{(0)}_{13}=\frac{2a\sinh\tilde{y}_{13}}{Z_{13}}, L^{(1)}_{13}=\frac{4a[2a+(1+a^2)\cosh\tilde{y}_{13}]}{Z^2_{13}},$$
$$P^{(0)}_{24}=\frac{1-a^2}{Z_{24}}, \quad P^{(1)}_{24}=\frac{-4a(1-a^2)\sinh\tilde{y}_{24}}{Z^2_{24}},$$
$$L^{(0)}_{24}=\frac{2a\sinh\tilde{y}_{24}}{Z_{24}}, \quad L^{(1)}_{24}=\frac{4a[2a+(1+a^2)\cosh\tilde{y}_{24}]}{Z^2_{24}},$$
$$Z_{13}=1+a^2+2a\cosh\tilde{y}_{13}; \quad Z_{24}=1+a^2+2a\cosh\tilde{y}_{24},$$

Substituting (3.6), (3.7) into equations (3.3), (3.4) and excluding parameters $\Delta_{ft}$, we obtained the following differential equations for the sums and differences of proton unary distribution functions:

$$\frac{d}{dt}\begin{pmatrix}\eta_{(1-3)t}\\ \eta_{(2-4)t}\end{pmatrix}=\begin{pmatrix}m^-_{11} & -m^-_{12}\\ -m^-_{21} & m^-_{22}\end{pmatrix}\begin{pmatrix}\eta_{(1-3)t}\\ \eta_{(2-4)t}\end{pmatrix} -\beta E_{1t}\begin{pmatrix}m_1\mu^x_{13}\\ -m_2\mu^x_{24}\end{pmatrix}. \quad (3.8)$$

$$\frac{d}{dt}\begin{pmatrix}\eta_{(1+3)t}\\ \eta_{(2+4)t}\end{pmatrix}=\begin{pmatrix}m^+_{11} & -m^+_{12}\\ -m^+_{21} & m^+_{22}\end{pmatrix}\begin{pmatrix}\eta_{(1+3)t}\\ \eta_{(2+4)t}\end{pmatrix} -\beta E_{2t}\begin{pmatrix}m_1\mu^y_{13}\\ -m_2\mu^y_{24}\end{pmatrix}. \quad (3.9)$$

$$\frac{d}{dt}\begin{pmatrix}\eta_{(1-3)t}\\ \eta_{(2-4)t}\end{pmatrix}=\begin{pmatrix}m^-_{11} & -m^-_{12}\\ -m^-_{21} & m^-_{22}\end{pmatrix}\begin{pmatrix}\eta_{(1-3)t}\\ \eta_{(2-4)t}\end{pmatrix} -\beta E_{3t}\begin{pmatrix}m_1\mu^z_{13}\\ m_2\mu^z_{24}\end{pmatrix}. \quad (3.10)$$

where

$$m^{\pm}_{11}=\frac{1}{\alpha}\big(1-\beta\nu^{\pm}_1r_{13}K_{13}\big),$$
$$m^{\pm}_{12}=\frac{1}{\alpha}[(1+K_{13})P^{(0)}_{13}+\beta\nu^{\pm}_2r_{13}K_{13}],$$
$$m^{\pm}_{21}=\frac{1}{\alpha}[(1+K_{24})P^{(0)}_{24}+\beta\nu^{\pm}_2r_{24}K_{24}],$$
$$m^{\pm}_{22}=\frac{1}{\alpha}\big(1-\beta\nu^{\pm}_3r_{24}K_{24}\big),$$
$$m_1=\frac{1}{\alpha}K_{13}r_{13}, \quad m_2=\frac{1}{\alpha}K_{24}r_{24},$$
$$K_{13}=\frac{P^{(1)}_{13}\tilde{\eta}_{13}+L^{(1)}_{13}}{2r_{13}-(P^{(1)}_{13}\tilde{\eta}_{13}+L^{(1)}_{13})}, r_{13}=1-\big(\tilde{\eta}_{13}\big)^2,$$
$$K_{24}=\frac{P^{(1)}_{24}\tilde{\eta}_{24}+L^{(1)}_{24}}{2r_{24}-(P^{(1)}_{24}\tilde{\eta}_{24}+L^{(1)}_{24})}, \ r_{24}=1-\big(\tilde{\eta}_{24}\big)^2.$$

Solving equations (3.8)–(3.10), we obtained the time-dependent mean values of the pseudospins of GPI. The components of the dynamic susceptibility of a GPI clamped crystal can be written as:

$$\chi_{11}(\omega)=\chi^0_{11}+\lim_{E_{1t}\to0}\frac{1}{\upsilon}\left[\mu^x_{13}\frac{d(\eta_{1t}-\eta_{3t})_1}{dE_{1t}}-\mu^x_{24}\frac{d(\eta_{2t}-\eta_{4t})_1}{dE_{1t}}\right], \quad (3.11)$$

$$\chi_{22}(\omega)=\chi^0_{22}+\lim_{E_{2t}\to0}\frac{1}{\upsilon}\left(\mu^y_{13}\frac{d(\eta_{1t}+\eta_{3t})_2}{dE_{2t}}-\mu^y_{24}\frac{d(\eta_{2t}+\eta_{4t})_2}{dE_{2t}}\right), \quad (3.12)$$

$$\chi_{33}(\omega)=\chi^0_{33}+\lim_{E_{3t}\to0}\frac{1}{\upsilon}\left(\mu^z_{13}\frac{d(\eta_{1t}-\eta_{3t})_3}{dE_{3t}}+\mu^z_{24}\frac{d(\eta_{2t}-\eta_{4t})_3}{dE_{3t}}\right), \quad (3.13)$$

The obtained susceptibilities consist of the "seed" part and two relaxational modes:

$$\chi_{ii}(\omega) = \chi^0_{ii} + \sum_{l=1}^{2} \frac{\chi^i_l}{1 + i\omega\tau^i_l},\ i = 1,2,3 \to (x,y,z) \quad (3.14)$$

where

$$\chi^i_l = \frac{\beta}{2v}\frac{\tau^i_1\tau^i_2}{\tau^i_2 - \tau^i_1}\{(-1)^{l-1}[(\mu^i_{13})^2 m_1 + (\mu^i_{24})^2 m_2]$$
$$+ (-1)^l \tau^i_l [(\mu^i_{13})^2 m_1 m^\gamma_{22} + (\mu^i_{24})^2 m_2 m^\gamma_{11}$$
$$- \mu^i_{13}\mu^i_{24}(m_1 m^\gamma_{21} + m_2 m^\gamma_{12})]\}, \quad (3.15)$$

where $\tau^i_{1,2}$ are the relaxation times of polarization, which have the following form:

$$(\tau^i_{1,2})^{-1} = \frac{1}{2}\{(m^\gamma_{11} + m^\gamma_{22}) \pm \quad (3.16)$$
$$\pm\sqrt{(m^\gamma_{11} + m^\gamma_{22})^2 - 4(m^\gamma_{11}m^\gamma_{22} - m^\gamma_{12}m^\gamma_{21})}\}.$$

In (3.15), (3.16) $\gamma$="+" for $i = y$ and $\gamma$="–" for $i = x, z$.

The components of the dynamic dielectric permittivity of the proton subsystem of GPI are as follows:

$$\varepsilon_{ii}(\omega) = 1 + 4\pi\chi_{ii}(\omega). \quad (3.17)$$

## IV. COMPARISON OF THE NUMERICAL CALCULATIONS WITH THE EXPERIMENTAL DATA. DISCUSSION OF THE OBTAINED RESULTS

To calculate the temperature, frequency and pressure dependences of the dynamic dielectric characteristics of GPI, we need to set certain values of the following the parameters: parameters of the short-range interactions $w^0$; the parameters of the long-range interactions $\nu^{0\pm}_f$ ($f$=1,2,3); deformational potentials $\delta_i$, $\psi^\pm_{fi}$ ($f$=1,2,3; $i$=1,...,6); effective dipole moments $\mu^x_{13}$; $\mu^x_{24}$; $\mu^y_{13}$; $\mu^y_{24}$; $\mu^z_{13}$; $\mu^z_{24}$; "seed" dielectric susceptibilities $\chi^{\varepsilon 0}_{ij}$, coefficients of piezoelectric stress $e^0_{ij}$ and elastic constants $c^{E0}_{ij}$.

The values of the given theory parameters are determined by studying of the static properties of GPI [2]: $w_0(x)/k_\mathrm{B} = 820\,\mathrm{K}$, $\tilde\nu^{0+}_1 = \tilde\nu^{0+}_2 = \tilde\nu^{0+}_3 = 2.643\,\mathrm{K}$, $\tilde\nu^{0-}_1 = \tilde\nu^{0-}_2 = \tilde\nu^{0-}_3 = 0.2\,\mathrm{K}$, where $\tilde\nu^{0\pm}_f = \nu^{0\pm}_f/k_\mathrm{B}$, $\tilde\delta_1 = 500\,\mathrm{K}$, $\tilde\delta_2 = 600\,\mathrm{K}$, $\tilde\delta_3 = 500\,\mathrm{K}$, $\tilde\delta_4 = 150\,\mathrm{K}$, $\tilde\delta_5 = 100\,\mathrm{K}$, $\tilde\delta_6 = 150\,\mathrm{K}$; $\tilde\delta_i$=$\delta_i/k_\mathrm{B}$;$\tilde\psi^+_{f1} = 87.9\,\mathrm{K}$, $\tilde\psi^+_{f2} = 237.0\,\mathrm{K}$, $\tilde\psi^+_{f3} = 103.8\,\mathrm{K}$, $\tilde\psi^+_{f4} = 149.1\,\mathrm{K}$, $\tilde\psi^+_{f5} = 21.3\,\mathrm{K}$, $\tilde\psi^+_{f6} = 143.8\,\mathrm{K}$, $\tilde\psi^-_{fi} = 0\,\mathrm{K}$, where $\tilde\psi^\pm_{fi}$ =$\psi^\pm_{fi}/k_\mathrm{B}$.

The effective dipole moments in the paraelectric phase are equal to $\mu^x_{13}$=$0.4{\cdot}10^{-18}$ esu·cm; $\mu^y_{13}$=$4.02{\cdot}10^{-18}$ esu·cm; $\mu^z_{13}$=$4.3{\cdot}10^{-18}$ esu·cm; $\mu^x_{24}$=$2.3{\cdot}10^{-18}$ esu·cm; $\mu^y_{24}$=$3.0{\cdot}10^{-18}$ esu·cm; $\mu^z_{24}$=$2.2{\cdot}10^{-18}$ esu·cm. In the ferroelectric phase, the $y$-component of the first dipole moment is $\mu^y_{13\mathrm{ferro}}(x) = 3.82\cdot10^{-18}$ esu·cm.

A majority of experimental measurements of thermodynamic characteristics were carried out for the samples with $T_c = 225\,\mathrm{K}$. Therefore, we chose the set of parameters from the condition of agreement of the calculated thermodynamic characteristics and the experimental data with $T_c = 225\,\mathrm{K}$. If we proportionally change the parameters $w^0$, $\nu^{0\pm}_f$, $\delta_i$, $\psi^\pm_{fi}$, $\mu^{x,y,z}_{13,24}$, than the temperature dependences of the calculated thermodynamic characteristics practically do not change, but only $T_c$ shifts proportionally to the change of these parameters. In the present paper, we use experimental data [10], where the transition temperature is $T_c = 223.6\,\mathrm{K}$, and the parameters $w^0$, $\nu^{0\pm}_f$, $\delta_i$, $\psi^\pm_{fi}$, $\mu^{x,y,z}_{13,24}$ should be multiply by coefficient $k = 223.6/225 \approx 0.994$.

The volume of the primitive cell of GPI is equal to $v = 0.601{\cdot}10^{-21}$ cm$^3$.

Parameter $\alpha$ is determined from the condition of agreement of the theoretically calculated and experimentally obtained frequency dependences of $\varepsilon_{22}(\omega)$. We consider that parameter $\alpha$ slightly changes with temperature:

$$\alpha = [1.6 - 0.011(\Delta T)]\cdot10^{-14}\,\mathrm{s}, \quad \Delta T = T - T_c.$$

The "seed" parameters $e^0_{ij} = 0.0\,\mathrm{esu}\cdot\mathrm{cm}^{-2}$;

$\chi^{\varepsilon 0}_{11} = 0.1$, $\chi^{\varepsilon 0}_{22}$= 0.403, $\chi^{\varepsilon 0}_{33} = 0.5$, $\chi^{\varepsilon 0}_{12} = \chi^{\varepsilon 0}_{13} = \chi^{\varepsilon 0}_{23} = 0.0$;

$c^{0E}_{11}$=$26.91\cdot10^{10}\,\mathrm{dyn}\cdot\mathrm{cm}^{-2}$, $c^{E0}_{12}$=$14.5\cdot10^{10}\,\mathrm{dyn}\cdot\mathrm{cm}^{-2}$, $c^{E0}_{13}$=$11.64\cdot10^{10}\,\mathrm{dyn}\cdot\mathrm{cm}^{-2}$, $c^{E0}_{15} = 3.91\cdot10^{10}\ \mathrm{dyn}\cdot\mathrm{cm}^{-2}$,

$c^{E0}_{22} = (64.99 - 0.04(T - T_c))\cdot10^{10}\,\mathrm{dyn}\cdot\mathrm{cm}^{-2}$, $c^{E0}_{23} = 20.38\cdot10^{10}\,\mathrm{dyn}\cdot\mathrm{cm}^{-2}$, $c^{E0}_{25} = 5.64\cdot10^{10}\,\mathrm{dyn}\cdot\mathrm{cm}^{-2}$,

$c^{E0}_{33} = 24.41\cdot10^{10}\,\mathrm{dyn}\cdot\mathrm{cm}^{-2}$, $c^{E0}_{35} = -2.84\cdot10^{10}\,\mathrm{dyn}\cdot\mathrm{cm}^{-2}$, $c^{E0}_{55} = 8.54\cdot10^{10}\,\mathrm{dyn}\cdot\mathrm{cm}^{-2}$,

$c^{E0}_{44} = 15.31\cdot10^{10}\,\mathrm{dyn}\cdot\mathrm{cm}^{-2}$, $c^{E0}_{46} = -1.1\cdot10^{10}\,\mathrm{dyn}\cdot\mathrm{cm}^{-2}$, $c^{E0}_{66} = 11.88\cdot10^{10}\,\mathrm{dyn}\cdot\mathrm{cm}^{-2}$.

Other components $c^{E0}_{ij} \equiv 0$.

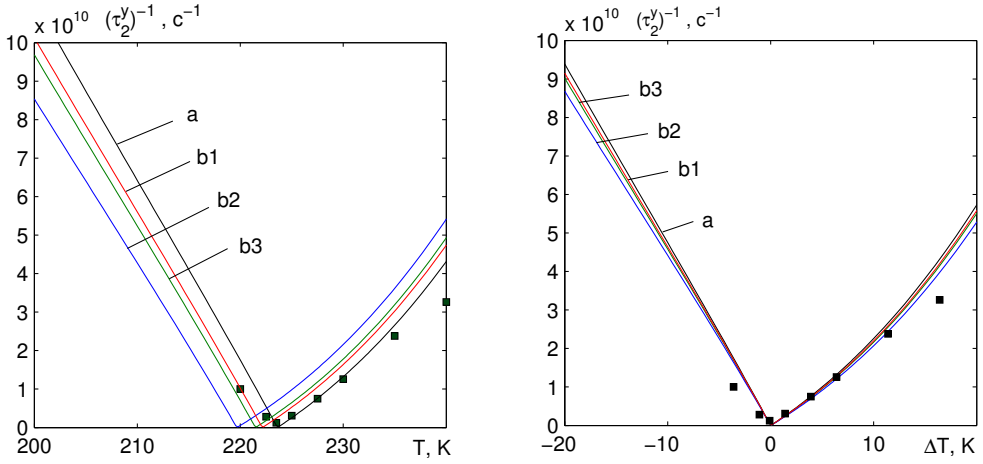


Fig. 2. (Color online). The temperature dependence of inverse relaxation time $(\tau_2^y)^{-1}$ at different directions of uniaxial pressure $p_i$ (i=1,2,3), and different values of pressure ($10^9$ dyn/cm$^2$): 0.0 — a, ■ [10]; 0.8 — b.

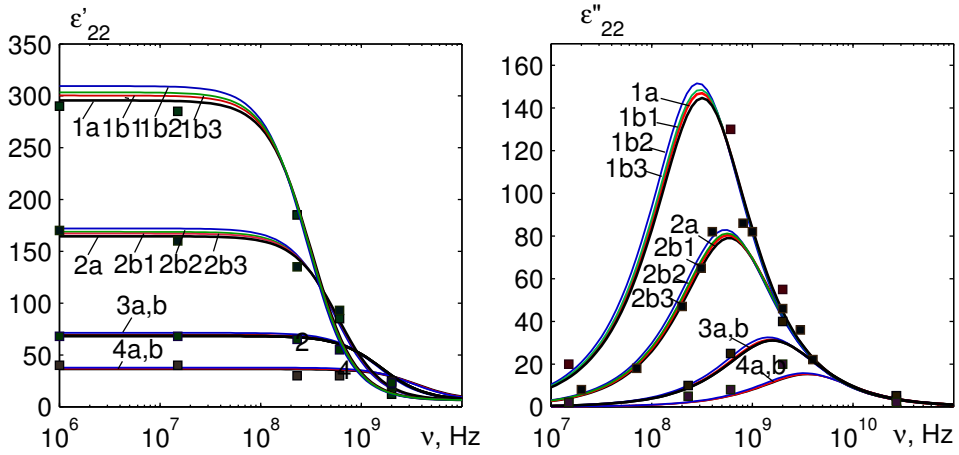


Fig. 3. (Color online). Frequency dependences of real $\varepsilon'_{22}$ and imaginary $\varepsilon''_{22}$ parts of the dielectric permittivity of GPI at different $\Delta T$ (K): 1.1 — 1; 2.0 — 2; 5.0 — 3; 10.0 — 4, at different directions of uniaxial pressure $p_i$ $(i = 1, 2, 3)$ and at different values of pressure ($10^9$ dyn $\cdot$ cm$^{-2}$): 0.0 — a, ■ [10] and 0.8 — b.

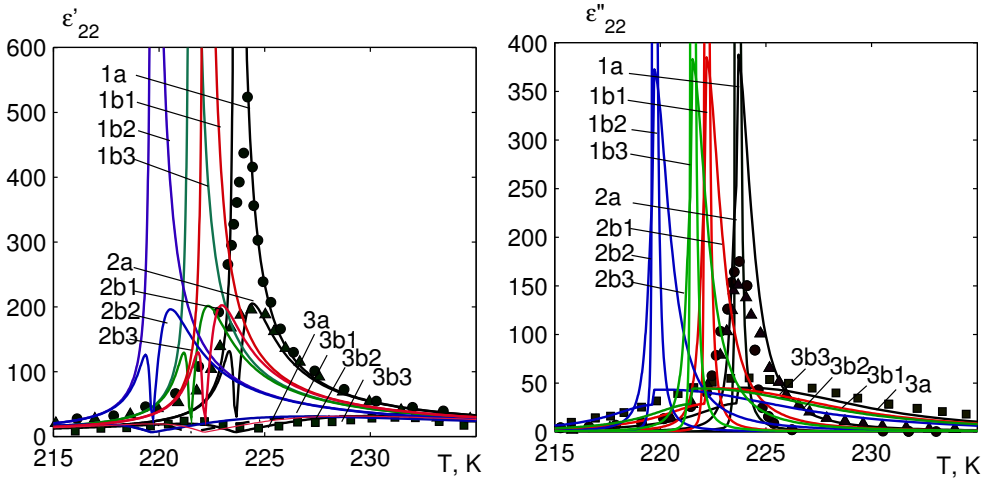


Fig. 4. (Color online). The temperature dependences of real $\varepsilon'_{22}$ and imaginary $\varepsilon''_{22}$ parts of the dielectric permittivity of GPI at different frequencies $\nu$ (GHz): 0.015 — 1, • [10]; 0.230 — 2,▲ [10]; 20.0 — 3,■ [10], at different directions of uniaxial pressure $p_i$ $(i = 1, 2, 3)$ and at values of pressure ($10^9$ dyn $\cdot$ cm$^{-2}$): 0.0 — a, 0.8 — b.

Let us now explain the obtained results. From expression (3.14) we can see that the dynamic dielectric characteristics depend on the behaviour of static dielectric characteristics $\chi_1^i, \chi_2^i$ and corresponding relaxation times $\tau_1^i$, $\tau_2^i$ in the system. Numerical analysis shows that only one contribution to the permittivities is determinative ($\chi_2^i \gg \chi_1^i$).

First, let us consider longitudinal dynamic dielectric characteristics. It was determined in [5] that uniaxial pressures decrease the phase transition temperature $T_c$ (which agrees with the experimental data [9]) and slightly increase the value of the static permittivity of our model at constant difference of temperature $\Delta T$.

The influence of uniaxial pressures on the relaxation time is illustrated in Fig. 2 on the temperature dependences of $(\tau_2^y)^{-1}$ at different values of pressures $p_i$.

Th vealue of $(\tau_1^y)^{-1}$ decreases when approaching the phase transition temperature and tends to zero at temperature $T = T_c$. As we can see from Fig. 2, uniaxial pressures $p_i$ decrease the phase transition temperature $T_c$ and decrease the value of $(\tau_1^y)^{-1}$ at constant $\Delta T$ (curves b1, b2, b3 correspond to pressures $p_1$, $p_2$, $p_3$, respectively) in comparison with $(\tau_1^y)^{-1}$ without pressure (curve a). We must note that in this figure and in all further figures the black color of the curves correspons to zero pressure, red — to pressure $p_1$, blue — to $p_2$, green — to $p_3$. Relaxation time $\tau_2^y$ is connected with some frequency typical of this crystal relaxation (soft relaxation mode) $\nu_s^y = (2\pi\tau_2^y)^{-1}$, which conventionally separates the regions of low-frequecy and high-frequency dynamics.

The influence of uniaxial pressures on dynamic permittivity can be seen best of all in the frequency dependences of real $\varepsilon'_{22}$ and imaginary $\varepsilon''_{22}$ parts of dielectric permittivity at different values of the temperature difference $\Delta T$ and at different values of the uniaxial pressures $p_i$ (Fig. 3).

The first digit on the designation of the curves is the number of $\Delta T$, the letters "a", "b", "c"... show the value of pressure, the last digit numbers the direction of applied pressure ($p_1$, $p_2$, $p_3$). The values of $\varepsilon'_{22}(\nu)$ and $\varepsilon''_{22}(\nu)$ under pressures (curves 1b1, 1b2, 1b3, 2b1, 2b2, 2b3) are higher than at zero pressure (curves 1a, 2a), owing to the increase in static permittivity at pressure. When $\Delta T$ decreases the region of dispersion shifts to lower frequencies owing to the increase in relaxation time when approaching $T_c$. Moreover, the curves $\varepsilon'_{22}(\nu)$ and $\varepsilon''_{22}(\nu)$ under pressures (curves 1b1, 1b2, 1b3, 2b1, 2b2, 2b3) make an additional shift to lower frequencies, due to an increase in relaxation time under pressures.

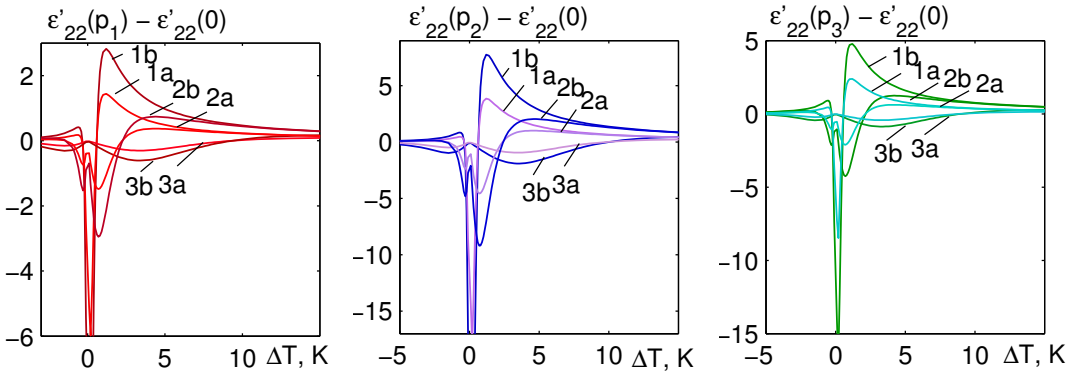


Fig. 5. (Color online). The temperature dependences of the differences of permittivity $\varepsilon'_{22}(p_i) - \varepsilon'_{22}(0)$ at different frequencies $\nu$ (GHz): 0.1 — 1; 0.4 — 2; 2.0 — 3, at different directions of uniaxial pressure $p_i$ ($i = 1, 2, 3$) and at different values of pressure ($10^9$ dyn $\cdot$ cm$^{-2}$): 0.4 — a; 0.8 — b.

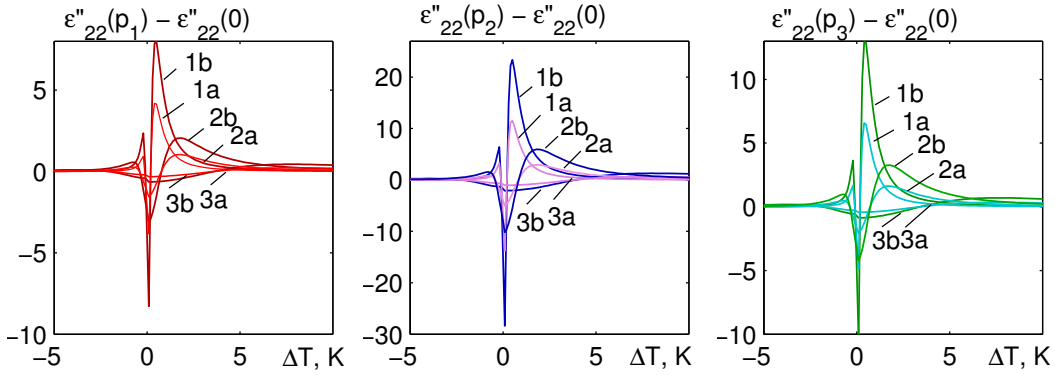


Fig. 6. (Color online). The temperature dependences of the differences of permittivity $\varepsilon''_{22}(p_i) - \varepsilon''_{22}(0)$ at different frequencies $\nu$ (GHz): 0.1 — 1; 0.4 — 2; 2.0 — 3, at different directions of uniaxial pressure $p_i$ ($i = 1, 2, 3$) and at different values of pressure ($10^9$ dyn $\cdot$ cm$^{-2}$): 0.4 — a; 0.8 — b.

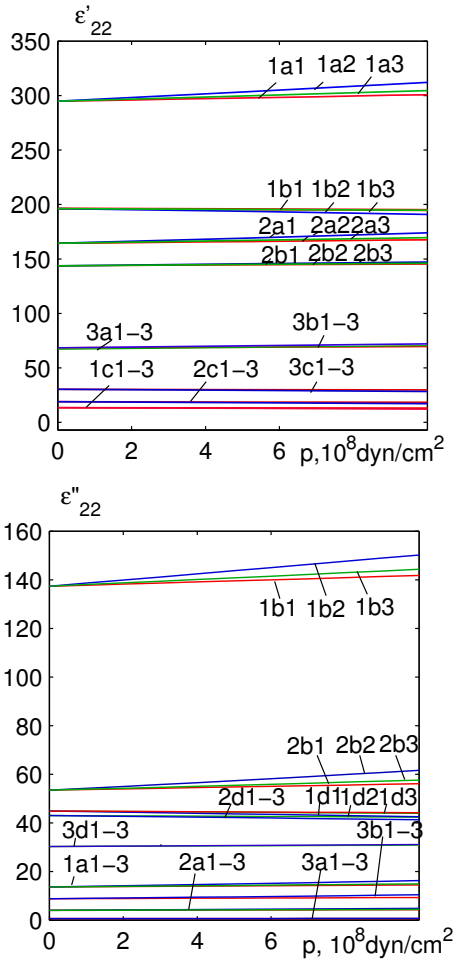


Fig. 7. (Color online). The pressure dependences of real $\varepsilon'_{22}$ and imaginary $\varepsilon''_{22}$ parts of the dielectric permittivity of GPI at different $\Delta T$ (K): 1.0 — 1; 2.0 — 2; 5.0 — 3, at different frequencies $\nu(10^9$ Hz): 0.015 — a; 0.230 — b; 0.610 — c; 20.0 — d and at different directions of uniaxial pressure $p_i$, $(i = 1, 2, 3)$.

The uniaxial pressures also manifest themselves in the temperature dependences of dynamic permittivity, mainly in the shift of curves $\varepsilon'_{22}(T)$ and $\varepsilon''_{22}(T)$ to the lower temperatures owing to the decrease in temperature $T_c$ with pressure (Fig. 4).

The curves of temperature dependences in this and further curves have the following designations. The first digit is the number of frequency, the letters "a", "b", "c"... show the value of pressure, the last digit numbers the direction of applied pressure ($p_1$, $p_2$, $p_3$). Moreover, at the temperatures far from $T_c$, the curves $\varepsilon'_{22}(T)$ are close to static (curves 1a, 1b1, 1b2, 1b3, and also 2a, 2b1, 2b2, 2b3 at large $\Delta T$) owing to small relaxation time, and therefore their values under pressures are larger than without pressure; imaginary parts $\varepsilon''_{22}(T)$ are close to zero. Such behaviour is more evident in the temperature dependences of the differences of permittivity under pressure and without pressure $\varepsilon_{22}(p_i) - \varepsilon_{22}(0)$ (Figs. 5, 6), where this difference is positive at large $\Delta T$.

When $\Delta T$ is small, curves $\varepsilon'_{22}(T)$ have lower values than static curves, and have a depression near $T_c$ owing to the large relaxation time; the imaginary part $\varepsilon''_{22}(T)$ has a peak near $T_c$. Since relaxation time increases with pressure, curves $\varepsilon'_{22}(T)$ under pressure have lower values than without pressure; the difference $\varepsilon'_{22}(p_i) - \varepsilon'_{22}(0)$ becomes negative (Fig. 5).

The influence of uniaxial pressures reveals itself in the pressure dependences of $\varepsilon'_{22}(p)$ and $\varepsilon''_{22}(p)$ (Fig. 7), in the increase in permittivity with pressure at low frequencies (curves 1ai, 2ai, 3ai, 2bi, 3bi for $\varepsilon'_{22}(p)$ and 1bi for $\varepsilon''_{22}(p)$), and also in the decrease of permittivity at high frequencies owing to the increase in relaxation time with pressure.

The first digit on the designation of the curves of pressure dependence is the number of $\Delta T$, the letters "a", "b", "c"... show the number of frequency, the last digit numbers the direction of applied pressure ($p_1$, $p_2$, $p_3$). It is necessary to note that the uniaxial pressure $p_2$ influences the calculated physical characteristics most evidently, while the pressure $p_1$ influences them least.

It is necessary to note that we do not take into account domain processes in our model. Therefore, we make no pretense to a good description of the dielectric dispersion in the low-frequency region in the ferroelectric phase.

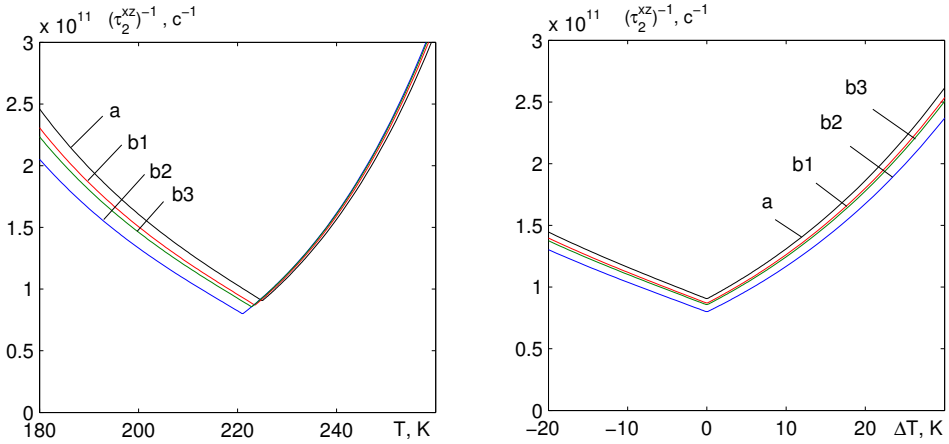


Fig. 8. (Color online). The temperature dependence of inverse relaxation time $(\tau_2^{xz})^{-1}$ at different directions of uniaxial pressure $p_i$ $(i = 1, 2, 3)$, and different values of pressure $(10^9 \mathrm{dyn/cm}^2)$: 0.0 — a, 0.8 — b.

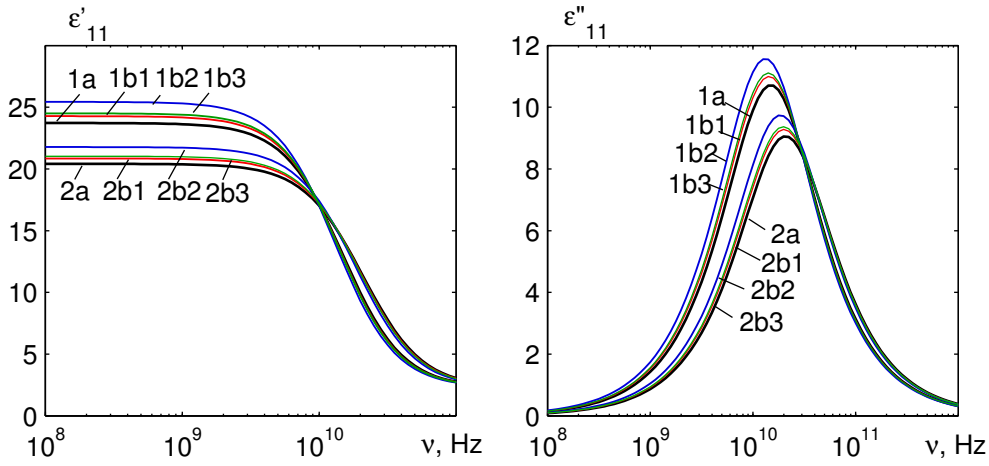


Fig. 9. (Color online). The frequency dependences of real $\varepsilon'_{11}$ and imaginary $\varepsilon''_{11}$ parts of the dielectric permittivity of GPI at different $\Delta T$ (K): 1 — 1; 10 — 2, at different directions of uniaxial pressure $p_i$ $(i = 1, 2, 3)$ and at different values of pressure ($10^9$ dyn $\cdot$ cm$^{-2}$): 0.0 — a, 0.8 — b.

Let us now siscuss the transverse dynamic characteristics. The designations of the curves are such as in the case of longitudinal dynamic characteristics. In [5] it was determined that the uniaxial pressure slightly increases the values of transverse static permittivity at constant temperature difference $\Delta T$. The influence of the uniaxial pressures on transverse relaxation times is presented in Fig. 8.

The transverse relaxation times $\tau_2^x$ and $\tau_2^z$ are calculated at the same $\alpha$ as the longitudinal time $\tau_2^y$. They are smaller than the longitudinal time and also increase when approaching the phase transition temperature. The transverse relaxation times $\tau_2^{x,z}$ in contrast to $\tau_2^y$ are finite at $T = T_c$. As one can see from Fig. 8, $\tau_2^{x,z}$ also increases under uniaxial pressures.

The frequency dependences of the real and imaginary parts of transverse dielectric permittivity $\varepsilon_{11}(\nu)$ (Fig. 9) and $\varepsilon_{33}(\nu)$ (Fig. 10) at different values of $\Delta T$ are qualitatively similar to the frequency dependences of $\varepsilon_{22}(\nu)$, but the region of dispersion exists at higher frequencies and changes with temperature more weakly.

The influence of uniaxial pressures on the frequency dependences of $\varepsilon_{11}(\nu)$ and $\varepsilon_{33}(\nu)$ is similar to the influence of these pressures on the longitudinal permittivities $\varepsilon_{22}(\nu)$. That is the curves $\varepsilon_{11}(\nu)$ and $\varepsilon_{33}(\nu)$ have larger values under pressures than at zero pressure and shift to lower frequencies owing to the increase in relaxation time with pressure.

The influence of uniaxial pressures on the temperature dependences of $\varepsilon_{11}(T)$ (Fig. 11) and $\varepsilon_{33}(T)$, (Fig. 12) is also similar to the influence of these pressures on the longitudinal permittivities $\varepsilon_{22}(T)$.

That is at low frequencies and at the temperatures far from $T_c$, curves $\varepsilon'_{11}(T)$ and $\varepsilon'_{33}(T)$ are close to the static ones (curves 1a, 1bi, and also 2a, 2bi at high $\Delta T$) due to the small relaxation time, and consequently, they have slightly larger values under pressures than without pressure. One can see this also from the temperature dependences of the difference of permittivities with and without pressures $\varepsilon_{11}(p_i) - \varepsilon_{11}(0)$ (Figs. 13 and 14). This difference is positive at large $\Delta T$.

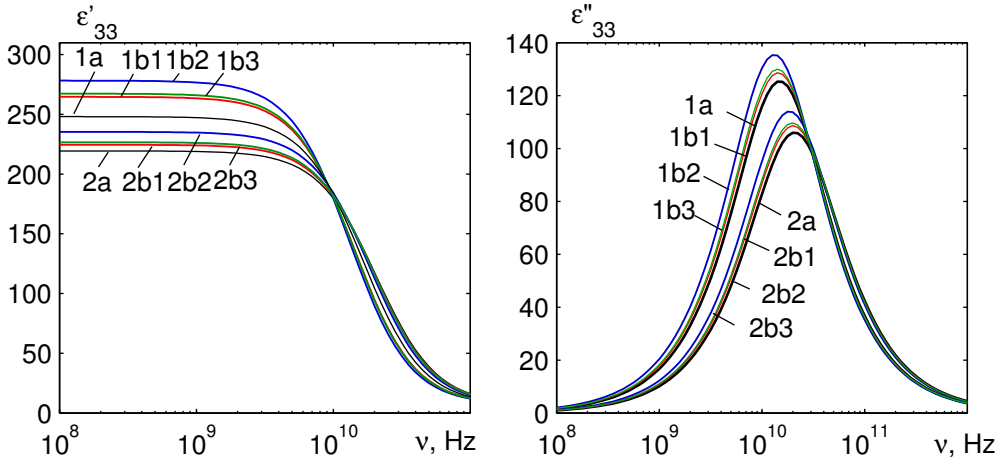


Fig. 10. (Color online). The frequency dependences of real $\varepsilon'_{33}$ and imaginary $\varepsilon''_{33}$ parts of the dielectric permittivity of GPI at different $\Delta T$ (K): 1 — 1; 10 — 2, at different directions of uniaxial pressure $p_i$ $(i = 1, 2, 3)$ and at different values of pressure ($10^9$ dyn $\cdot$ cm$^{-2}$): 0.0 — a, 0.8 — b.

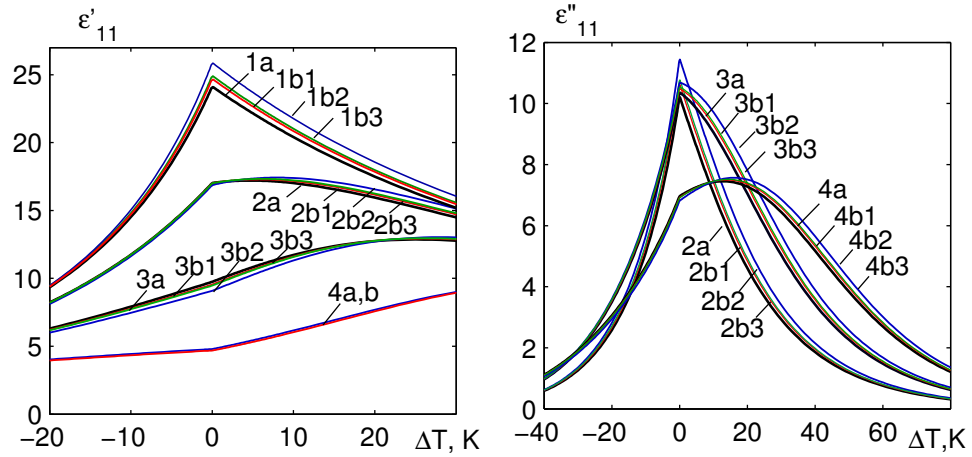


Fig. 11. (Color online). The temperature dependences of real $\varepsilon'_{11}$ and imaginary $\varepsilon''_{11}$ parts of the dielectric permittivity of GPI at different frequencies $\nu$ (GHz): 0 — 1; 10 — 2; 20 — 3; 40 — 4, at different directions of uniaxial pressure $p_i$ $(i = 1, 2, 3)$ and at different values of pressure ($10^9$ dyn $\cdot$ cm$^{-2}$): 0.0 — a, 0.8 — b.

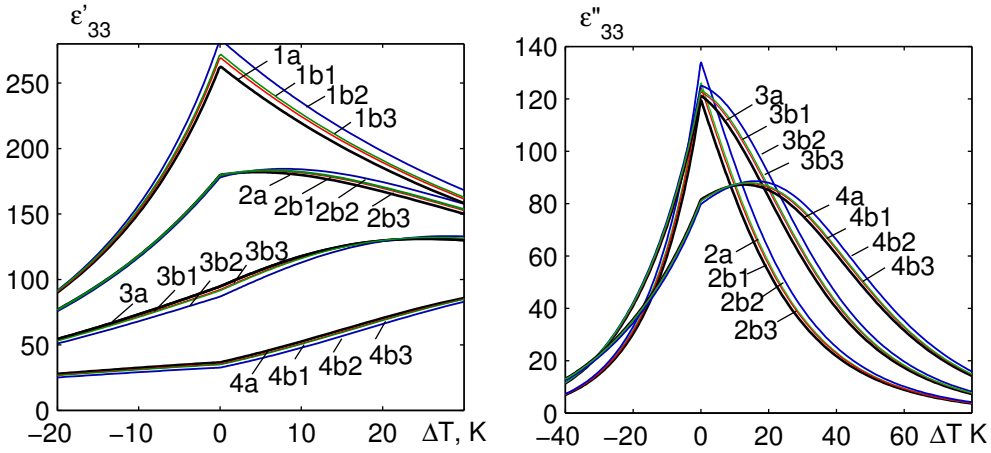


Fig. 12. (Color online). The temperature dependences of real $\varepsilon'_{33}$ and imaginary $\varepsilon''_{33}$ parts of the dielectric permittivity of GPI at different frequencies $\nu$ (GHz): 0 — 1; 10 — 2; 20 — 3; 40 — 4, at different directions of uniaxial pressure $p_i$ $(i = 1, 2, 3)$ and at different values of pressure ($10^9$ dyn $\cdot$ cm$^{-2}$): 0.0 — a, 0.8 — b.

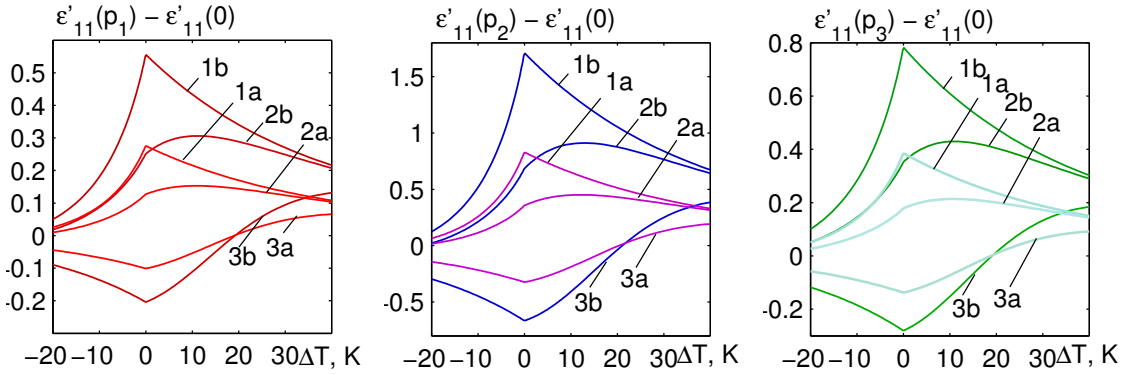


Fig. 13. (Color online). The temperature dependences of the difference $\varepsilon'_{11}(p_i) - \varepsilon'_{11}(0)$ at different frequencies $\nu$ (GHz): 1.0 — 1; 6.0 — 2; 20.0 — 3, at different directions of uniaxial pressure $p_i$ $(i = 1, 2, 3)$ and at different values of pressure ($10^9$ dyn $\cdot$ cm$^{-2}$): 0.4 — a; 0.8 — b.

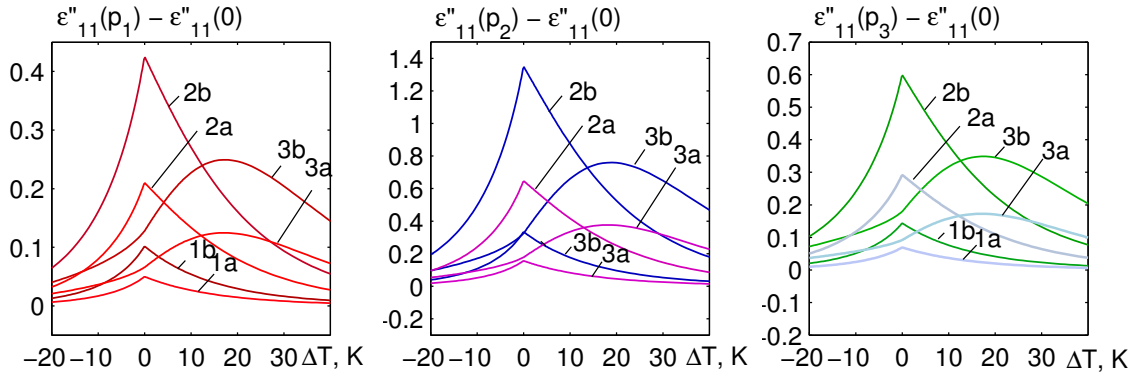


Fig. 14. (Color online). The temperature dependences of the difference $\varepsilon''_{11}(p_i) - \varepsilon''_{11}(0)$ at different frequencies $\nu$ (GHz): 1.0 — 1; 6.0 — 2; 20.0 — 3, at different directions of uniaxial pressure $p_i$ $(i = 1, 2, 3)$ and at different values of pressure ($10^9$ dyn $\cdot$ cm$^{-2}$): 0.4 — a; 0.8 — b.

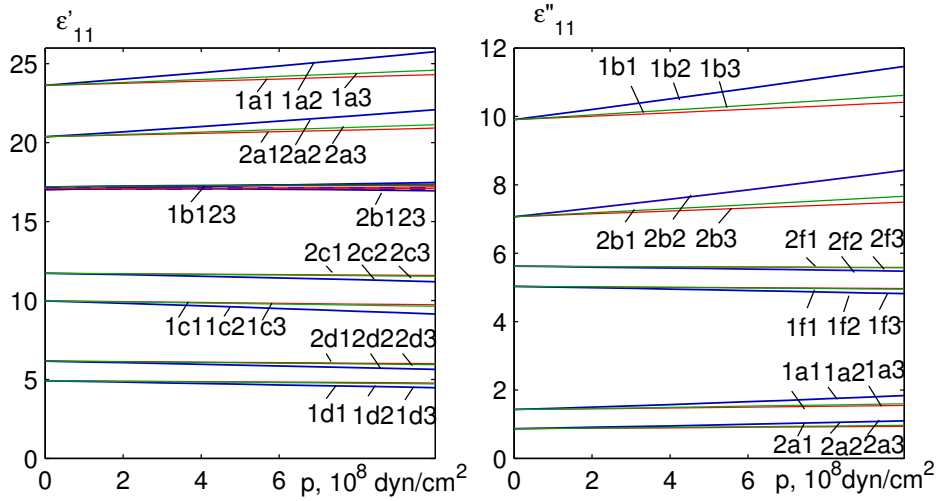


Fig. 15. (Color online). The pressure dependences of real $\varepsilon'_{11}$ and imaginary $\varepsilon''_{11}$ parts of the dielectric permittivity of GPI at different $\Delta T$ (K): 1 — 1; 10 — 2, at different frequencies $\nu$ (GHz): 1.0 – a; 10.0 — b; 20.0 — c; 40.0 — d; 60.0 — f, and at different directions of uniaxial pressure $p_i$, $(i = 1, 2, 3)$.

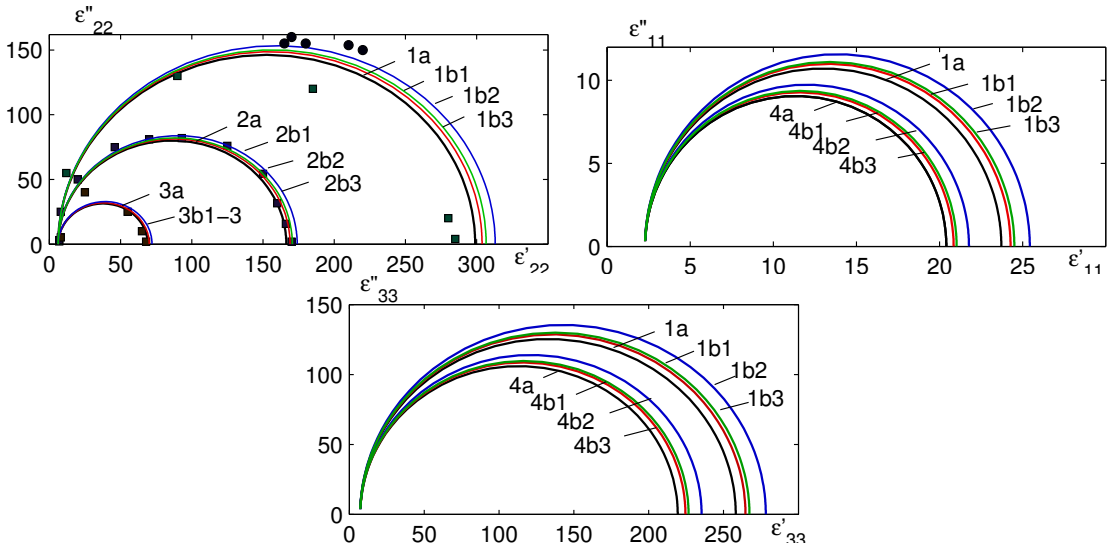


Fig. 16. (Color online). Cole–Cole curves at different $\Delta T$ (K):1.0 — 1, ■ [10], • [11]; 2.0 — 2, ■ [10]; 5.0 — 3, ■ [10]; 10.0 — 4, at different directions of uniaxial pressure $p_i$ $(i = 1, 2, 3)$ and at different values of pressure ($10^9$ dyn $\cdot$ cm$^{-2}$): 0.0 — a; 0.8 — b.

When approaching the temperature $T_c$, the relaxation time increases; as a result, the curves $\varepsilon'_{11}(T)$ and $\varepsilon'_{33}(T)$ increasingly bend down; but imaginary parts $\varepsilon''_{11}(T)$ and $\varepsilon''_{33}(T)$ increase. Since the relaxation time increases with pressure, the curves $\varepsilon'_{11}(T)$ and $\varepsilon'_{33}(T)$ have lower values under pressure than without pressure.

The pressure dependences of real $\varepsilon'_{11}$ and imaginary $\varepsilon''_{11}$ parts of the dielectric permittivity of GPI at different $\Delta T$ and at a different frequencies $\nu$ are presented in Fig. 15.

The character of the pressure dependences of real $\varepsilon'_{33}$ and imaginary $\varepsilon''_{33}$ parts of the dielectric permittivity of GPI is analogous to the pressure dependences of $\varepsilon'_{11}$ and $\varepsilon''_{11}$, but the numerical values of $\varepsilon_{33}$ are $\sim 10$ times larger then $\varepsilon_{11}$. An increase in uniaxial pressures leads to a linear increase in permittivities $\varepsilon'_{11}$ and $\varepsilon'_{33}$ at high $\Delta T$ and pre-relaxational frequencies. But in the region of relaxational frequencies the permittivities practically do not change. At higher frequencies the transverse permittivities slightly decrease with pressures.

The results of calculation of Cole–Cole curves at different $\Delta T$ with and without uniaxial pressures (Fig. 16) show monodispersivity of the dielectric permittivities of GPI.

Some disagreement with experimental data at $\Delta T = 1$ K may be connected with the low measurement accuracy near $T_c$. In all cases, the radii of Cole–Cole semi-circles increase when approaching the $T_c$ and with an increase in pressures.

## V. CONCLUSIONS

The influence of uniaxial pressures on the dielectric properties of GPI reveals itself in a decrease of the phase transition temperature an increase in static dielectric permittivities and an increase in relaxation times. This leads to an increase in dynamic dielectric permittivity under pressures at the pre-relaxation frequencies and the shift of the dispersion region to lower frequencies. The dynamic longitudinal and transverse permittivities have a monodispersive character. Uniaxial pressures have a weak influence on the relaxation dynamics of the proton subsystem of GPI. The effect of the uniaxial pressure $p_2$ on the calculated physical characteristics is the strongest, and the effect of the pressure $p_1$ is the weakest. Our model does not take into account domain processes and cannot describe well the dielectric dispersion in the low-frequency region in the ferroelectric phase. The obtained results have a predictive character and can stimulate subsequent experimental investigations.

[1] I. Stasyuk, Z. Czapla, S. Dacko, O. Velychko, Condens. Matter Phys. **6**, 483 (2003).
[2] I. R. Zachek, Ya. Shchur, R. R. Levitskii, A. S. Vdovych, Physica B **520**, 164 (2017).
[3] I. R. Zachek, R. R. Levitskii, A. S. Vdovych, I. V. Stasyuk, Condens. Matter Phys. **20**, 23706 (2017).
[4] I. R. Zachek, R. R. Levitskii, A. S. Vdovych. Condens. Matter Phys. **20**, 43707 (2017).
[5] I. R. Zachek, R. R. Levitskii, A. S. Vdovych, J. Phys. Stud. **21**, 1704 (2017).
[6] I. R. Zachek, R. R. Levitskii, A. S. Vdovych, O. B. Bilenka, Condens. Matter Phys. **21**, 13704 (2018).
[7] J. Glauber, J. Math. Phys. **4**, 294 (1963).
[8] I. V. Stasyuk, R. R. Levitskii, A. P. Moina, A. G. Slivka, O. V. Velychko, *Field and deformational effects in complex ferroelectric compounds* (Grazhda, Uzhgorod, 2009).
[9] T. Kikuta, Y. Takemoto, T. Yamazaki, N. Nakatani, Ferroelectrics **99**, 302 (2004).
[10] R. Tchukvinskyi *et al.*, Acta Phys. Polonica A **92**, 1191 (1997).
[11] R. Sobiestianskas, A. Brilingas, Z. Czapla, J. Korean Phys. Soc. **32**, S377 (1998).

## ДВПЛИВ ОДНОВІСНИХ ТИСКІВ НА ДИНАМІЧНІ ВЛАСТИВОСТІ СЕҐНЕТОЕЛЕКТРИКА $NH_3CH_2COOH{\cdot}H_2PO_3$

І. Р. Зачек[1], Р. Р. Левицький[2], А. С. Вдович[2]
[1] *Національний університет "Львівська політехніка", вул. С. Бандери, 12, Львів, 79013, Україна*
[2] *Інститут фізики конденсованих систем НАН України, вул. Свенціцького, 1, Львів, 79011, Україна*

Використовуючи модифіковану модель $NH_3CH_2COOH{\cdot}H_2PO_3$ і врахувавши п'єзоелектричний зв'язок із деформаціями $\varepsilon_i$, методом Ґлаубера в наближенні двочастинкового кластера отримано систему кінетичних рівнянь для середніх значень псевдоспінів. На основі розв'язків цих рівнянь розраховано залежні від температури, частоти і тисків компоненти тензора динамічної діелектрисної проникності кристала GPI. Вивчено вплив одновісних тисків на ці характеристики за різних частот і температур.